Saudi Pharmaceutical Journal 32 (2024) 102154

HOSTED BY

Contents lists available at ScienceDirect

Saudi Pharmaceutical Journal

journal homepage: www.sciencedirect.com

Original article

Mannosylated PAMAM G2 dendrimers mediated rate programmed delivery of efavirenz target HIV viral latency at reservoirs

Rohini Kharwade [a], Mohsin Kazi [b], Nilesh Mahajan [a,*], Payal Badole [a], Sachin More [c], Asaad Kayali [d], Md Noushad Javed [e], Mohammed Kaleem [c,**]

[a] Department of Pharmaceutics, Dadasaheb Balpande College of Pharmacy, Besa, Nagpur, Rashtrasant Tukadoji Maharaj Nagpur University, Nagpur, MS, India
[b] Department of Pharmaceutics, College of Pharmacy, King Saud University, P.O. Box 2457, Riyadh 11451, Saudi Arabia
[c] Department of Pharmacology, Dadasaheb Balpande College of Pharmacy, Rashtrasant Tukadoji Maharaj Nagpur University, Nagpur, Maharashtra 440037, India
[d] Department of Biomedical Sciences, College of Health Science, Abu Dhabi University, Abu Dhabi P.O. Box 59911, United Arab Emirates
[e] NationNanotechnology Center of Excellence, College of Engineering and Computer Science, The University of Texas Rio Grande Valley, Edinburg, TX, USA

ARTICLE INFO

Keywords:
PAMAM G2
Mannose conjugation
Efavirenz
Ritonavir
Viral reservoir
Targeted drug delivery

ABSTRACT

In this current research, we conceptualized a novel nanotechnology-enabled synthesis approach of targeting HIV-harboring tissues via second-generation (G2) polyamidoamine (PAMAM) mannosylated (MPG2) dendrimers for programmed delivery of anti-HIV drugs efavirenz (EFV) and ritonavir (RTV). Briefly, here mannose served purpose of ligand in this EFV and RTV-loaded PAMAM G2 dendrimers, synthesized by divergent techniques, denoted as MPG2ER. The developed nanocarriers were characterized by different analytical tools FTIR, NMR, zeta potential, particle size, and surface morphology. The results of confocal microscopy showed substantial alterations in the morphology of H9 cells, favored by relatively higher drug uptake through the MPG2ER. Interestingly, the drug uptake study and cytotoxicity assay of MPG2ER demonstrated that it showed no significant toxicity up to 12.5 μM. A typical flow cytometry histogram also revealed that MPG2ER efficiently internalized both drugs, with an increase in drug uptake of up to 81.2 %. It also enhanced the plasma pharmacokinetics of EFV, with C_{max}7.68 μg/ml, AUC of 149.19 (μg/ml) * hr, and MRT of 26.87 hrs. Subsequently, tissue pharmacokinetics further evidence that MPG2ER accumulated more in distant Human immunodeficiency virus (HIV) reservoir tissues, such as the lymph nodes and spleen, but without exhibiting significant toxicity. Abovementioned compelling evidences strongly favored translational roles of MPG2 as a potential therapeutic strategy in the clinical eradication of HIV from viral reservoir tissue.

1. Introduction

Human immunodeficiency virus (HIV) is a single-stranded (ss) RNA enveloped retrovirus; belongs to *lentivirus* family. Among the majority of HIV cases, HIV-1 is primarily responsible for the worldwide AIDS pandemic (Seitz, 2016). HIV propagation requires active CD4 host cells. Once viral gp120 adheres to the host CD4 receptor, it forms a CD4-gp120-chemokine receptor complex (Rojekar et al, 2021a). Through this complex, the viral particle enters the cell and initiates the virus cycle (Rojekar et al, 2021b).

Several factors are responsible for managing HIV infection, including latent viral reservoir sites. These sites are inaccessible for various drugs and drug delivery systems owing to contribution of several factors, more particularly inadequate perfusion of drugs to the specific tissues and elimination of therapeutic moieties via P-gp efflux pumps. Highly active antiretroviral therapy (HAART) with two or three classes of drugs is also not effective at delivering a sufficient concentration of drugs and is therefore inefficient at controlling infection. Suitable concentrations of

* Corresponding author at: Department of Pharmaceutics, Dadasaheb Balpande College of Pharmacy, Rashtrasant Tukadoji Maharaj Nagpur University, Nagpur, MS 440037, India.
** Corresponding author at: Department of Pharmacology, Dadasaheb Balpande College of Pharmacy, Rashtrasant Tukadoji Maharaj Nagpur University, Nagpur, Maharashtra, 440037, India.
E-mail addresses: rohinismore1@gmail.com (R. Kharwade), mkazi@ksu.edu.sa (M. Kazi), nmmahajan78@gmail.com (N. Mahajan), payalbadole09@gmail.com (P. Badole), sam007more@gmail.com (S. More), asaadkayali@hotmail.com (A. Kayali), rxnoushad@gmail.com (M. Noushad Javed), kaleemmubin88@gmail.com (M. Kaleem).

https://doi.org/10.1016/j.jsps.2024.102154
Received 23 March 2024; Accepted 7 August 2024
Available online 13 August 2024

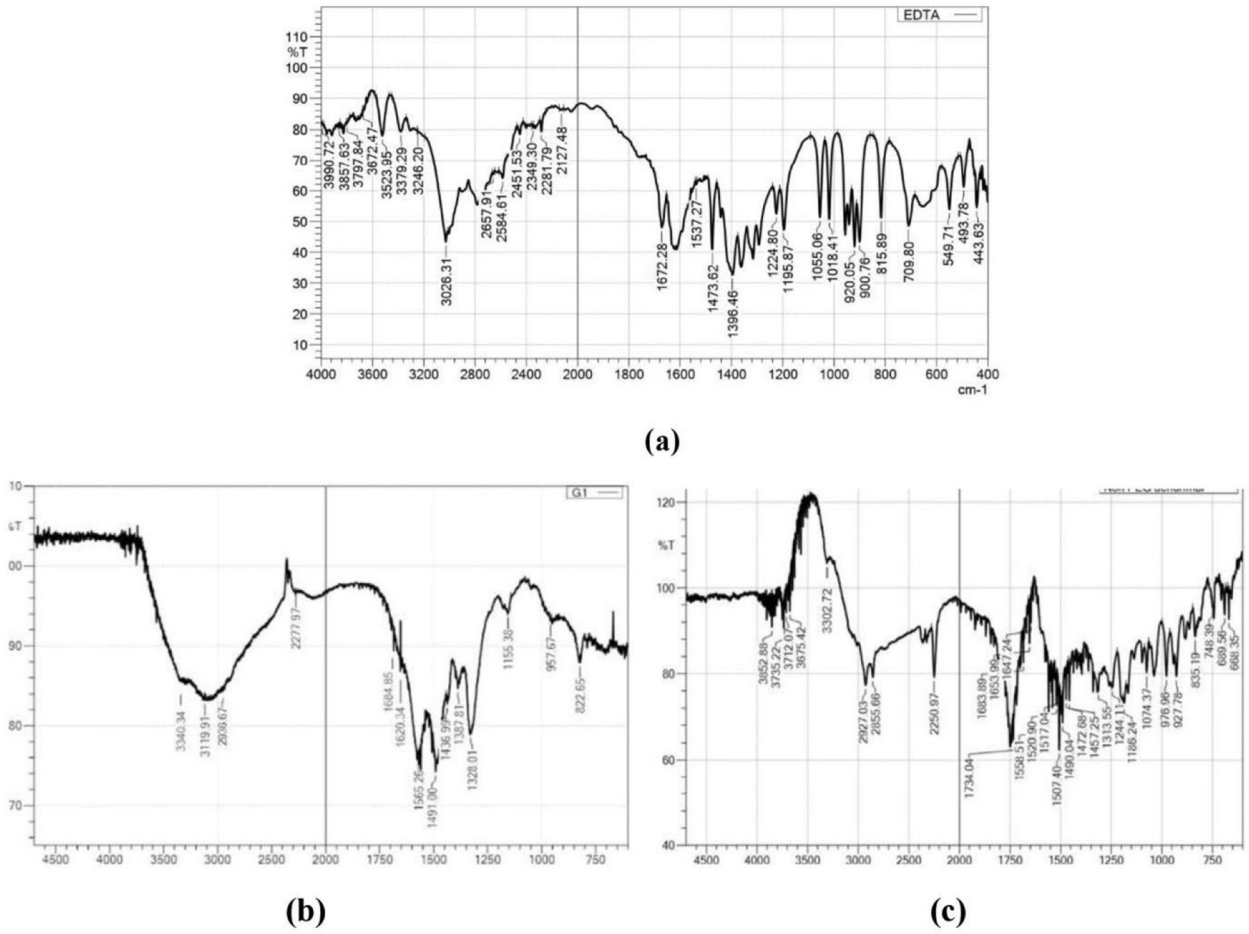

Fig. 1. FTIR spectrum of starting material EDTA (a), PG2(b) and mannosylated PG2 (MPG2) (c). The absorption band of specific functional groups confirmed the synthesis of PG2 and MPG2.

antiretroviral drugs cannot reach dormant viral reservoirs (Nelson et al, 2015). Therefore, targeting latent virus reservoirs with ligand-attached nanocarriers would be more effective at achieving high intracellular concentrations with lower toxicity (Iannazzo et al, 2015). Polyamidoamine (PAMAM) dendrimer nanocarriers can block HIV from attaching to host cells. These has been investigated for their significant interventions towards *trans*-activator transcription (Tat) protein bindings towards the *trans*-acting responsive element (TAR) of HIV-RNAs. PAMAM dendrimers also reported to disrupt the gp120-CD4 complex and may prevent HIV from entering cells (Peng et al, 2013; Kharwade et al, 2020a).

Subsequently, HIV has a greater affinity for the dendritic cell ICAM-3-grabbing integrin (DC-SIGN). These cells have pattern recognition C-type lectin receptors (CLRs) with affinity for carbohydrate moieties. Therefore, DC-SIGN cells function as receptors with greater affinity for the mannose-α1 and 2-mannose motifs on viral gp120 (Jin et al, 2014).

Therefore, mannose has been used as a ligand conjugated with PAMAM dendrimers for targeting DC-SIGN receptors. Thus, this whole nanocarrier cargo could be more intensively attached to target HIV reservoir dendritic cells. This modified PAMAM prevents host dendritic cells (DCs) from interacting with the virus gp120 and aids in targeting reservoir tissue accumulation (Filipczak et al, 2021; Kharwade et al, 2021). Accordingly, mannosylated PAMAM dendrimers are an attractive option for increasing therapeutic effectiveness and lowering the toxicity of antiretroviral formulations (Dutta & Jain, 2007; Filipczak et al, 2021).

EFV is the first-line nonnucleoside reverse transcriptase inhibitor used in current drug regimens for anti-HIV therapy. However, owing to limited bioavailability and fast metabolic rate of EFV, critically a very high dose is critical requirement for the optimal performance in clinics. However, such a high dose are not only increase cost of the treatments because of expensive HIV moieties, but it further lead to persistent dose mediated side effects, more particularly of central nervous system (CNS). Therefore, a trend has been emerged to integrate RTV as a suggested booster dose, in combination with EFV, to favor increased bioavailability of EFV. Moreover, RTV increases the bioavailability of EFV by 21 % by inhibiting CY450 3A4 (Kappelhoff et al, 2004).

Currently, there are no clinical remedies available in the market for targeting HIV viral harbor tissues to reduce latency and effectively irradiate the virus from reservoirs. However, few market drugs available in market EFV but used for the treatment of HAART, to reduce initial viral load. Kaletra is a combinational product of lopinavir and ritonavir which is used to reduce viral load (Hull & Montaner, 2011; Pau & George, 2014). Hence, owing to facts that during highly effective antiretroviral therapy (HAART), HIV mostly remains latent in the spleen and lymph nodes, wherein mannose ligands have preferential affinity towards the DC-SIGN receptor dendrimer cargo.

Hence, we reported a novel nanotechnology enabled strategy for designing mannosylated PAMAM G2 dendrimers, for targeted co-delivery of EFV in presence and booster RTV, in abovementioned pathological tissue compartments which reported improved PK profile and enhanced clinical promises towards eradication of HIV.

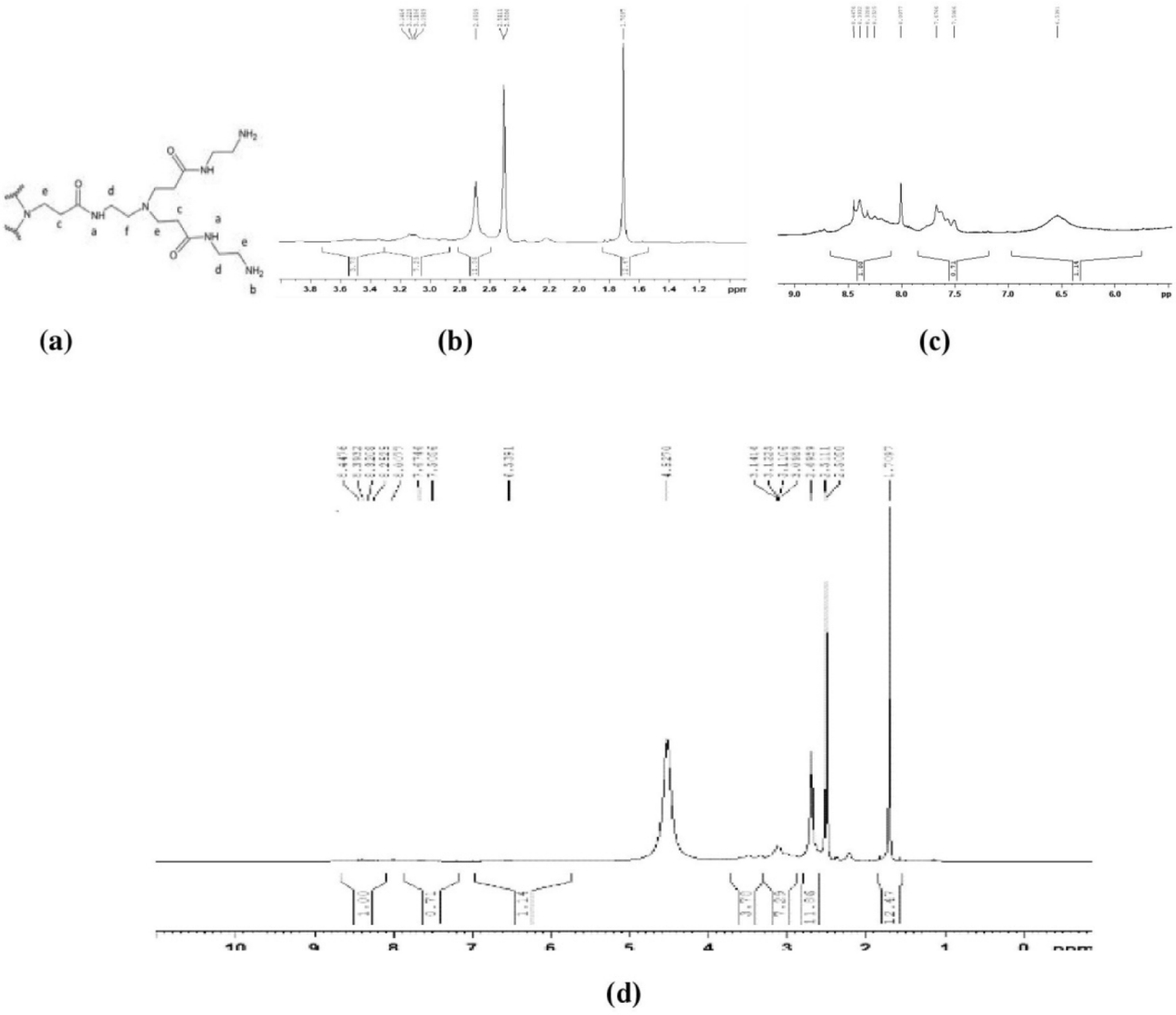

Fig. 2. Proton nuclear magnetic resonance (^{1}H NMR) spectrum of PG2 with its partial structure (a) and mannosylated PG2 (b).

2. Materials

2.1. Chemicals

The drugs EFV, RTV, and darunavir (DRV) were obtained from Emcure Pharmaceuticals Ltd., Ahmedabad, India. HPLC-grade acetonitrile, methanol, acetic acid and water were purchased from Loba Chemie Pvt. Ltd., Mumbai, India. Cell culture medium: RPMI-1640 media supplemented with 10 % (v/v) fetal bovine serum (FBS) (Sigma–Aldrich, Louis, MO, Cat No: RM10432) was purchased from Thermo Fisher-Gibco Life Technologies (Cat No: 11875093). An Annexin-V FITC/PI kit and Triton X 100 were obtained from Guava Technologies Inc., Hayward, CA, USA, and Sisco Research Laboratories Pvt Ltd., Mumbai, respectively. The cellulose dialysis bag MWCO 12–14 Kda, 3-(4,5-dimetylthaizol-2–2-y1)- 2,5-diphenyl) tetrazolium bromide (MTT reagent) (Cat No: 4060), and 0.45 μm membrane filter paper was obtained from Himedia Labs, Mumbai, India. 5-Fluorouracil (Cat No: F6627), DMSO (PHR 1309), and all other chemicals were obtained from Sigma Aldrich (St. Louis, MO, USA).

2.2. Animals

Male Wistar rats were sanctioned for pharmacokinetics and tissue distribution studies of MPG2ER (IAEC Ref: DBCOP/IAEC/1426/21–22/P2:P5). All rats were 200 ± 50 g in weight and kept in an environmentally controlled breeding room with access to standard laboratory food and water. Twenty-four hours before the experiment, the tested rats were fasted overnight.

2.3. Cell culture and treatment

The H9 cell line (human embryonic stem cell line) was obtained from the American Type Culture Collection (NCCS Pune, India). The cells were maintained in RPMI1640 media supplemented with 10 % (v/v) fetal bovine serum (FBS), 2 mM glutamine, the antimycotic agent (50 μg/L) and streptomycin (Sigma–Aldrich, St. Louis, MO, USA; 100 μg/ml). All cell lines were maintained in a humidified incubator containing 5 % CO_2 at 37 °C and sub-cultured every 2 days. The H9 cell suspension was grown in a T25 flask by the thawing method and checked after 24–48 hrs under an inverted biological microscope (Alghamdi et al, 2020; Michniak-Kohn et al, 2022).

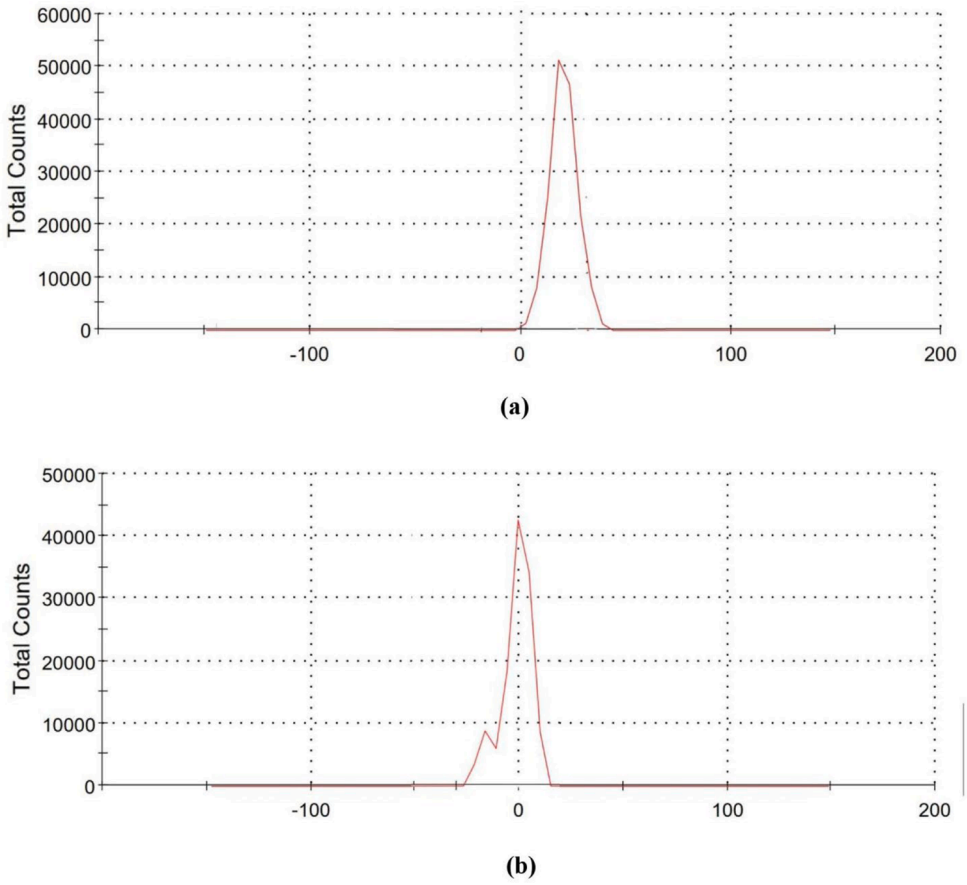

Fig. 3. Zeta potential of PG2 (a) and mannosylated PG2 (MPG2) (b). Surface modification with d-mannose has significantly decreased the value of zeta potential up to 0.267 mV and transformed PG2 into a unionized form.

3. Methods

3.1. Synthesis of PAMAM G2 (PG2)

The divergent technique was used in the synthesis of PG2 dendrimers. Subsequently, each synthesized product was purified using azeotropic distillation as reported earlier. Zeta potential (Malvern Instrument, Malvern, UK.), FTIR (DRS 8000A Shimadzu, Japan.), and ^{1}H NMR (Bruker Avance Neo 500 MHz NMR spectrometer, with D_2O as a solvent, Switzerland) were used to determine the charge, functional group, and proton group location, respectively (Kharwade et al, 2022).

3.2. Mannosylation of PAMAM G2 (MPG2)

To reduce its intrinsic hematotoxicity, cationic charge and steric hindrance, the terminal amine groups of PAMAM must have surfaces modified by d-mannose (Zhang et al, 2011). The mannosylation of PG2 is also preferable for DC-SIGN binding(Jain et al, 2010).

With agitation, 1 g of PG2 (0.000305 M) was solubilized in 1 % aqueous acetic acid at a pH of 5.5. An aqueous solution of 0.5 g of sodium tri-acetoxy borohydride (0.00244 M) and 0.44 g d-mannose (0.00244 M) was prepared separately. The resulting viscous PG2 solution was then mixed with the above solution by slow stirring and allowed to rest for 48 hrs at room temperature. Then, it was dialyzed against double distilled water (MWCO 12–14 kDa; Himedia, India) for 72 hrs and lyophilized (Chaubey & Mishra, 2014). Furthermore, it was noted as MPG2 and characterized by FTIR, NMR, and zeta potential.

3.3. Preparation of EFV-RTV-loaded mannosylated PAMAM G2 (MPG2ER)

An earlier reported method was used for drug entrapment in MPG2 with a dendrimer-to-drug ratio of 1:1 w/w (Kharwade et al, 2022, 2023). The mixture of drugs contained 10 mg of EFV-RTV in a 4:1%w/w ratio. The produced yellow powder was lyophilized and again characterized by FTIR to determine the drug nanocarrier interaction, % drug content, % drug loading, FE-SEM (JSM-6380A Scanning Electron Microscope; 200kv; JEOL Ltd., Japan.) for morphological determination and TEM (JEM-2100 Plus Electron Microscope; 200 kV; JEOL Ltd.; Japan) for the determination of the particle size and drug entrapment.

3.4. In vitro drug release study

The *in-vitro* drug release of EFV and RTV from MPG2ER was investigated by dialysis. An equivalent concentration of 10 mg/ml (EFV-RTV) containing MPG2ER was dissolved in 5 ml of phosphate buffer (PBS; 100 mM; pH 7.4). It was transferred to a dialysis bag and put into a beaker containing 50 ml of phosphate buffer. The experiment was carried out under sink conditions at 37 °C with slow magnetic stirring. At intervals of 0, 1, 1.5, 2, 4, 6, 12, 18, 24, 48, 72, 96, and 120 hr, 1 ml aliquots were collected for analysis and compensated with the same volume of fresh PBS solution. The concentrations of both drugs present in the aliquot at different time intervals were monitored by HPLC (Photodiode array detector; LC-20 AD Shimadzu, Japan.) at 254 nm (Michniak-Kohn et al, 2022). The same procedure was repeated in acetate buffer (pH 4; 10 mM) to determine the % drug release (n = 3).

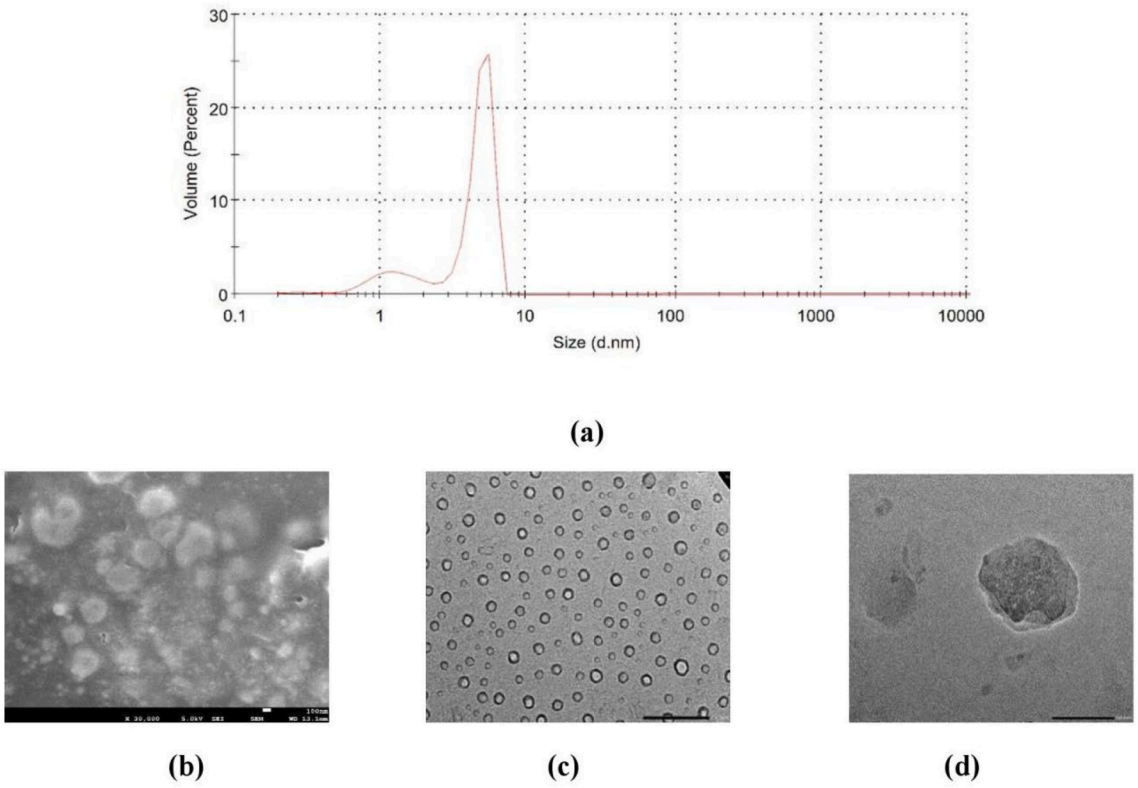

Fig. 4. The particle size of MPG2ER 7.75 nm with PDI 0.047 was observed (a). The Morphological image of FE-SEM (b) and TEM (c) and (d) showed that particles were uniformly spherical with a nanosize range.

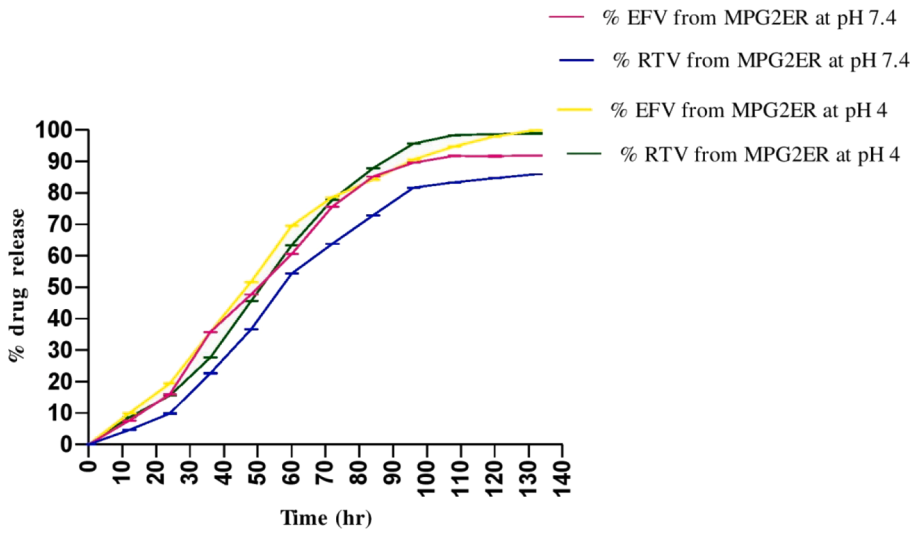

Fig. 5. In vitro drug release of EFV and RTV from MPG2ER at pH 4 and pH 7.4. It showed that the release rate was lower at pH 7.4 as compared to pH 4. The PAMAM dendrimers were mentioned as having the greatest potential for drug release in an HIV-infected physiological condition.

Table 1a
Release kinetics of EFV from MPG2ER.

Sr. No	Formulation	pH	Zero Order (R^2)	First Order (R^2)	Higuchi Model (R^2)	Korsmeyes-Peppas Model (R^2)	EFV release exponent (n)
1	MPG2ER	7.4	0.861	0.967	0.976	0.958	0.587
2	MPG2ER	4	0.850	0.963	0.971	0.956	0.585

Table 1b
Release kinetics of RTV from MPG2ER.

Sr. No	Formulation	pH	Zero Order (R^2)	First Order (R^2)	Higuchi Model (R^2)	Korsmeyes-Peppas Model (R^2)	RTV release exponent (n)
1	MG2ER	7.4	0.881	0.970	0.980	0.967	0.615
2	MG2ER	4	0.872	0.977	0.983	0.966	0.604

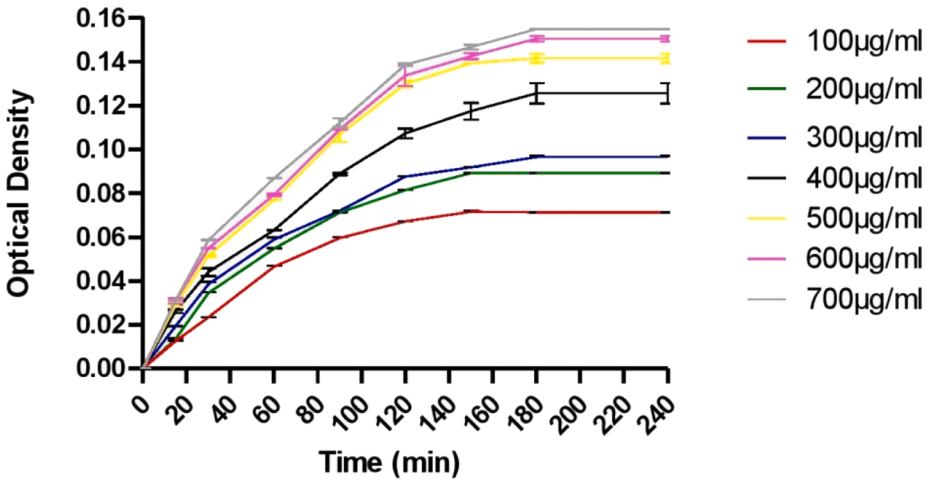

Fig. 6. Time and concentration of Con A dependent in vitro ligand agglutination assay of MPG2ER.

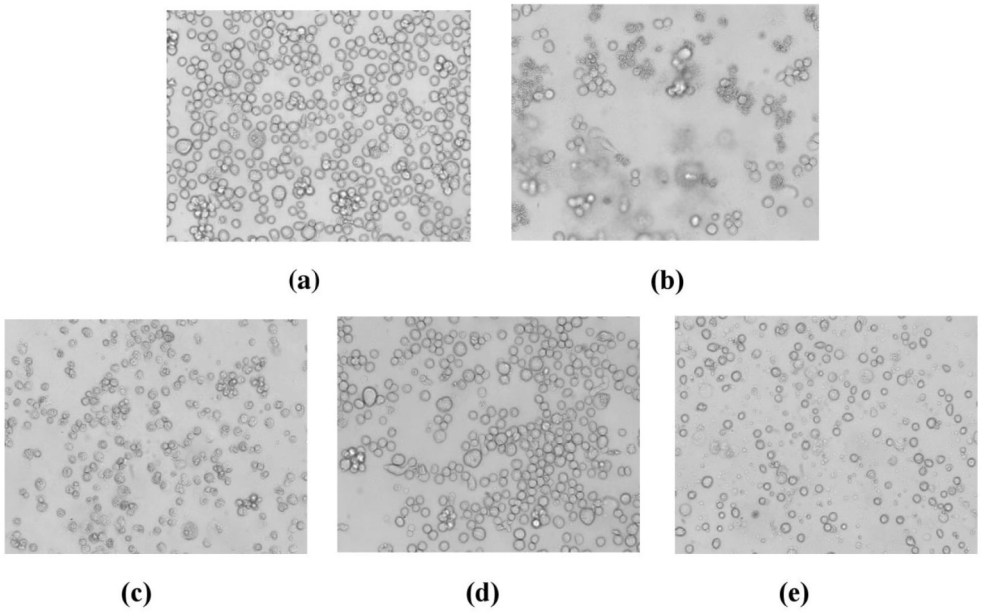

Fig. 7. Cell viability of H9 cells of untreated (a) and after the treatment with EFV-RTV (b), PG2 (c), MG2 (d), and MPG2ER (e).

3.5. Ligand agglutination assay

MPG2ER was tested for in-vitro ligand binding by using mannose-binding Con A. One hundred microliters of a 10 % aqueous solution of MPG2ER was diluted in 10 ml of PBS and transferred to 7 test tubes, each containing 1 ml of MPG2ER solution. Furthermore, 1 mM manganese chloride, 1 mM calcium chloride and 1 ml of Con A in PBS (concentrations ranging from 100-700 µg/L) were added to the above MPG2ER solutions. The solution mixture was stored at 25 °C for up to 4 hrs. The intensity of turbidity with respect to time was noted down to 4 hrs by spectrophotometric monitoring at 550 nm (Dutta & Jain, 2007).

3.6. MTT assay

Cell viability MTT assay method was adopted to estimate the cytotoxic level of MPG2ER. Initially, H9 cells were incubated and subcultured in 96-well plates as described earlier. After 24 hrs, the density of the cells in each well was observed. When the density of cells in each well was $1x10^4$, the cells were exposed to EFV-RTV (4:1 w/w), PG2, MPG2, or MPG2ER at concentrations of 10, 5, 2.5, 1.25, or 0.625 µM/ml. The optical density was quantified at 550 nm utilizing a microplate ELISA reader (ELx800™; BioTek Instruments, Inc.) and Gen 5 software (BioTek Instruments, Inc.). Metabolically active cells

Table 2
Cell viability and IC50 value with immune H9 after treatment of EFV-RTV, MPG2, MPG2ER.

Sr.No	Sample	Concentration (μM/mL)	% Cell viability	IC50 (μg/mL)
1	EFV-RTV	100	42.56 ± 1.361	59.48
		50	64.15 ± 0.892	
		25	87.08 ± 2.340	
		12.50	97.86 ± 2.033	
		6.25	98.81 ± 1.821	
2	PG2	100	39.15 ± 0.942	42.79
		50	43.23 ± 1. 086	
		25	69.87 ± 1.411	
		12.50	85.43 ± 2.334	
		6.12	92.31 ± 1.701	
3	MPG2	100	42.02 ± 1.745	75.94
		50	55.63 ± 1. 380	
		25	75.97 ± 2.011	
		12.50	89.13 ± 2.532	
		6.12	98.21 ± 2.032	
4	MPG2ER	100	45.62 ± 2.076	76.27
		50	54.03 ± 1. 782	
		25	76.27 ± 2.033	
		12.50	91.83 ± 2.136	
		6.12	97.01 ± 2.821	

Note: All values are represented as mean ± SD (n = 3).

transform the color of yellow tetrazolium into purple formazan crystals. The percentage of cell viability of treated cells was quantified by in terms of comparing with reference to the control sample (Michniak-Kohn et al, 2022; Fule et al, 2023).

3.7. Confocal analysis

For confocal microscopy analysis, H9 cells (2x 10^5 cells/well per test) were seeded in 24-well culture plates. The plates were covered with sterile coverslips that had been treated with poly-L-ornithine solution (0.01 %). The cells were then incubated in the presence of 5 % CO_2 (Thermo Scientific, Inc., USA) with 200 μL of EFV-RTV (10 μM/ml) and MPG2ER (equivalent amount of EFV-RTV 10 μM/ml) for 24 hrs in the dark at 37 ± 1 °C. Furthermore, the cells were rinsed three times with saline (pH 7.4) and preserved in 4 % paraformaldehyde with PBS. Subsequently, the membrane was permeabilized with 0.1 % Triton TM X-100 in PBS and stained with ethidium bromide (EtBr) (for binding to the cytoskeleton) and acridine orange (AO) (for binding to nucleic acids). Later, the coverslips were washed, dried and mounted through dibutyl-phthalate polystyrene xylene (DPX). The cells were imaged for EtBr at 560/40 nm and 645/75 nm for excitation and emission, respectively. AO was also imaged at 470/40 nm and 525/50 nm for excitation and emission, respectively (Heidegger et al, 2015).

3.8. Flow cytometry

An Annexin-V FITC/propidium iodide (PI) kit (Guava Technologies Inc., Hayward, CA, USA) was used to conduct the apoptosis assay. Phosphatidylserine (PS) is a membrane component that is normally found on the internal face of a cell. Annexin-V FITC is a calcium-dependent binding protein dye that has a high affinity for PS. H9 cells were cultured for 24 hrs in 96-well plates at a density of 4 × 10^4 cells per well (Park et al, 2017). Furthermore, the cells were exposed to 10 μM/ml EFV-RTV or MPG2ER for 24 hrs at 37 ± 1 °C in 5 % CO_2. The cells were then washed with PBS, trypsinized, and centrifuged at 1000 rpm, and the supernatant was discarded. The cells were incubated for 15 min by adding 5 μL of annexin binding buffer. Then, 10 μL of annexin-binding buffer was added to 2.5 μL of annexin-V/FITC, and the mixture was incubated for another 15 min in the dark. Finally, the cells were washed twice with 1 ml of PBS, fixed in 400 μl of 1 % PI and analyzed using a FACS Calibur flow cytometer with BD Cell Quest Pro software 2.7.2. In this study, three cell types were distinguished as follows:

- Nonapoptotic cells: Annexin V (−) and PI (−)
- Early apoptotic cells: Annexin V (+) and PI (−)
- Late apoptotic cells: Annexin V (+) and PI (+) (Kaleem et al, 2024).

3.9. In vivo bioavailability and tissue distribution study

Eighty-four male Wistar rats were used to assess the in vivo bioavailability and tissue distribution pharmacokinetic parameters. All rats were randomly divided into three groups: the control group,

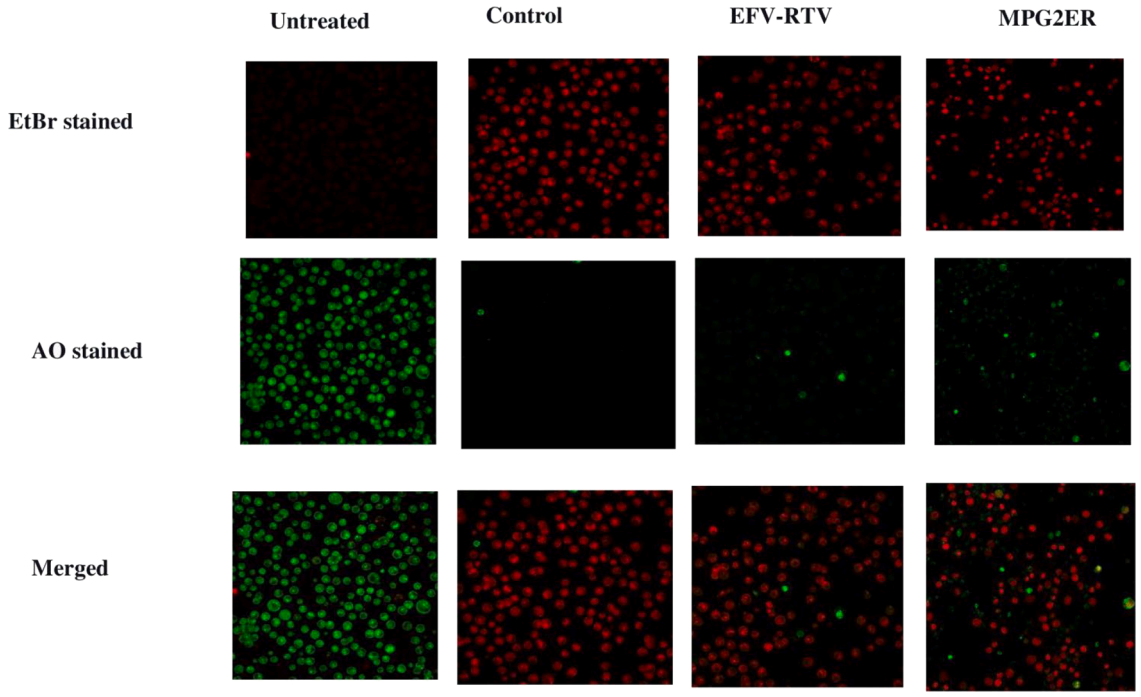

Fig. 8. The EFV-RTV and MPG2ER treatments induced significant apoptotic morphological alteration in H9 cells observed with respect to EtBr and AO staining.

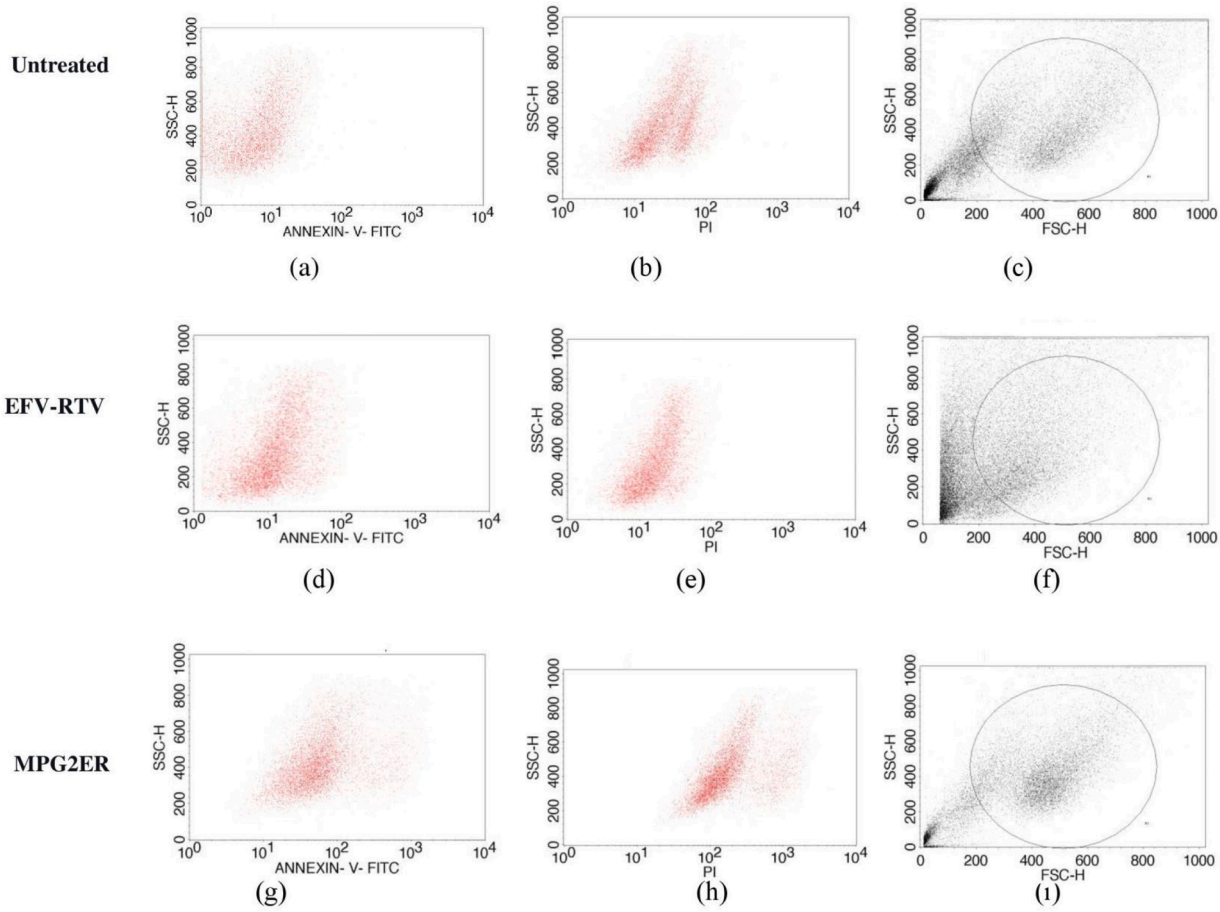

Fig. 9. A typical FSC-SSC double scatter plot graph together with the fluorescence intensity distribution of cells exposed to 10 μM/ml EFV-RTV and MPG2ER for 24 hrs.

standard group and test group. The control group contained 4 rats, the standard group treated with EFV-RTV-free drug contained 40 rats, and the MPG2ER-treated test group contained 40 rats. The standard group and test group rats were subdivided into ten groups, each containing 4 rats (Kharwade et al, 2022, 2023). EFV-RTV and MPG2ER were prepared in 5 % v/v dimethyl sulfoxide (DMSO) at a dose equivalent to 10 mg/kg. The dose was administered by the intraperitoneal route in a fasted state.

After dosing, 0.5 ml blood samples were withdrawn from the *retro*-orbital plexus at intervals of 0.5, 1, 2, 4, 6, 12, 24, 48, 72, and 96 hrs. Instantaneously, all the samples were centrifuged for 10 min at 12000 rpm at 4 °C. Furthermore, plasma was decanted from all samples, subjected to single-step protein precipitation and analyzed by HPLC at 254 nm (Makwana et al, 2015). As previously reported, the concentrations of both drugs in blood plasma and tissue homogenates were determined using a bioanalytical method (Kharwade et al, 2022).

At the aforementioned time intervals, the rats were euthanized by cervical dislocation for tissue distribution. Kidney, lymph node, brain, liver, and spleen tissues were removed, homogenized, subjected to single-step protein precipitation and assessed by HPLC to determine the drug concentration in the tissue.

3.10. Histopathology study

The complete microscopic analysis of all the organ tissues, as revealed by tissue distribution (the EFV-RTV- and MPG2ER-treated groups), was performed after 12 hrs via histopathological analysis. For this, we used the same method as that described in our earlier publication (Kharwade et al, 2023).

3.11. Stability studies

A stability study of MPG2ER was performed by keeping the 10 ml sample under an ambered and transparent glass bottle. The samples were placed at 0 °C, room temperature or accelerated temperature (60 ± 2 °C) for up to 6 weeks (Michniak-Kohn et al, 2022). The stored samples were evaluated initially and intermittently for up to 6 weeks for consistency, drug content, color or any turbidity. The drug release was also investigated throughout storage duration. The method was repeated for ~ 6 weeks, to determine the optimal storage conditions.

4. Results

4.1. Synthesis and characterization of PG2 and MPG2

PG2 dendrimers were synthesized using a divergent synthesis technique with an excess of reagents. A copper sulfate chelation test was performed to verify each step of the synthesis. The half-generation exhibited a dark blue color, whereas the full generation of PAMAM displayed a purple color.

The FTIR spectra of the EDTA and PG2 dendrimers are shown in Fig. 1 **(a) and (b),** respectively, which confirmed all the functional groups in the PG2 structure with respect to the starting material EDTA**.** After mannosylation, the free hydroxyl group of the asymmetric carbon of mannose showed peaks at 2855.66 cm^{-1}(Pyreddy et al, 2014) and 2250.97 cm^{-1} at the ends of the oligomer chain, as shown in Fig. 1(c).

The synthesis of PG2 was further confirmed by proton nuclear magnetic resonance (^{1}H NMR) spectroscopy, as shown in Fig. 2 **(b) and (c)**. The presence of all resonating signals with respect to the partial

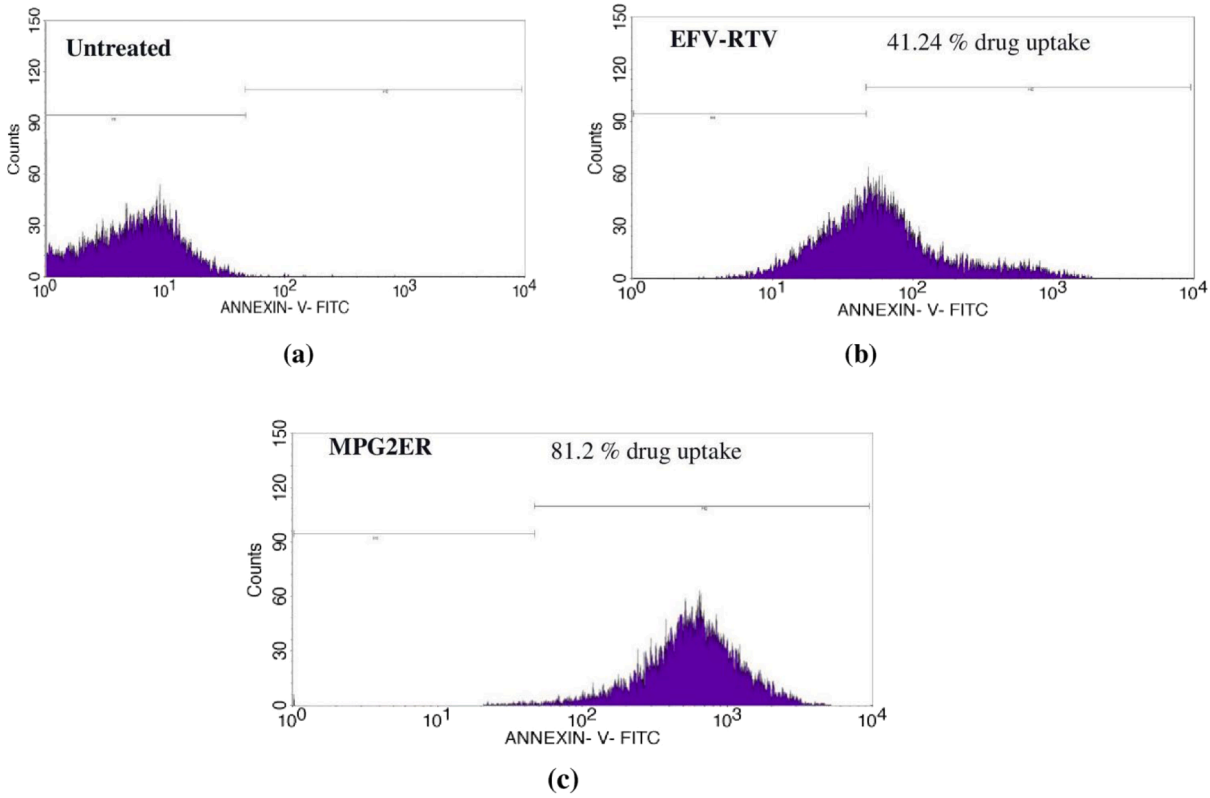

Fig. 10. Typical histogram of flow cytometry results for untreated cells and cells exposed EFV-RTV, MPG2ER, the distribution of cell fluorescence shifts to higher values as compared to EFV-RTV as results cells taking up PAMAM dendrimers loaded EFV-RTV more effectively.

Table 3a
Pharmacokinetic parameters for EFV and RTV in plasma after the treatment of MPG2ER.

Sr. No	Parameters	MPG2ER(RTV)	MPG2ER (EFV)
1	C_{max} (µg/mL)	1.95 ± 0.062	7.68 ± 0.121
2	t_{max} (hr)	6	6
3	$t_{1/2}$ (hr)	15.77 ± 0.671	19.09 ± 0.890
4	MRT (hr)	20.81 ± 0.912	26.87 ± 0.654
5	AUC_{tol} (µg/mL)*hr	31.30 ± 1.053	149.19 ± 2.052
6	AUMC (µg/mL)*hr	651.41 ± 10.272	4008.46 ± 21.350
7	Cl (µg/kg)/((µg/mL)/hr	0.07 ± 0.010	0.06 ± 0.010
8	Vss (mg.kg)/hr	1.81 ± 0.020	1.699 ± 0.031

Note: All values are represented as mean ± SD (n = 3).

Table 3b
Pharmacokinetic parameters for EFV and RTV in plasma after the treatment of EFV-RTV.

Sr. No	Parameters	EFV-RTV (RTV)	EFV-RTV (EFV)
1	C_{max} (µg/mL)	1.13 ± 0.041	3.64 ± 0.053
2	t_{max} (hr)	4	6
3	$t_{1/2}$ (hr)	10.14 ± 0.702	8.60 ± 0.032
4	MRT (hr)	12.23 ± 0.721	19.84 ± 0.03
5	AUC_{tol} (µg/mL)*hr	15.84 ± 1.034	111.83 ± 0.131
6	AUMC (µg/mL)*hr	241.38 ± 12.343	1608.65 ± 10.981
7	Cl (µg/kg)/((µg/mL)/hr	0.15 ± 0.011	3.13 ± 0.012
8	Vss (mg.kg)/hr	2.30 ± 0.030	0.65 ± 0.020

Note: All values are represented as mean ± SD (n = 3).

structure of PG2 (Fig. 2 **(a))** in the ^{1}H NMR spectrum confirmed the synthesis of PG2. The results of the mannosylation of PG2 showed that the isopropylidene protons of the oligomers resonated at approximately δ1.70 ppm, which was not lost during the polycondensation of d-mannose with PG2 (Shadrack et al, 2018). Additionally, the signals at δ 7.50 ppm indicated that the aromatic proton was protected by a benzyl moiety. The methylene groups in the mannose are indicated by the signal at δ 4.50, as shown in Fig. 2 **(d).**

The zeta potential of PG2 was found to be + 17.16 mV, as shown in Fig. 3 **(a).** Cationic charge on PG2 dendrimers due to the presence of 16 NH_2 groups. However, surface functionalization by d-mannose neutralizes the charge of PG2, and the zeta potential decreases to + 0.267 mV, as shown in Fig. 3 **(b),** which supports the transformation of PG2 to its unionized form.

4.2. Characterization of EFV and RTV-loaded mannosylated PG2 (MPG2ER)

The % drug content in MPG2ER was estimated to be 89.62 ± 0.044 % for EFV and 87.52 ± 0.104 % for RTV. The entrapment efficiencies of MPG2 for EFV and RTV were found to be 89.03 ± 1.874 % and 86.20 ± 0.914 %, respectively. The particle size of the MPG2ER nanoformulation was 7.75 nm, with a polydispersity index of 0.047, as depicted in Fig. 4 (a).

FE-SEM images of the MPG2ER particles are shown in Fig. 4 **(b)**. The particles were slightly aggregated, were uniformly spherical, and ranged in size from 7 to 10 nm. Two layers with nearly monodisperse and rounded shapes could be separated in a typical TEM image of the MPG2ER, which is represented in Fig. 4 **(c) and (d)**. The drug was encapsulated in MPG2 as suggested by the inner layer.

4.3. In vitro drug release study

Phosphate buffer (PBS, pH 7.4) and acetate buffer (pH 4) were used to determine the in vitro drug release from the MPG2ER formulation, as shown in Fig. 5. The obtained release concentration of the drug demonstrated that the rate of drug release was lower in PBS than in pH 4. Its greatest potential for drug release in HIV-infected cells was

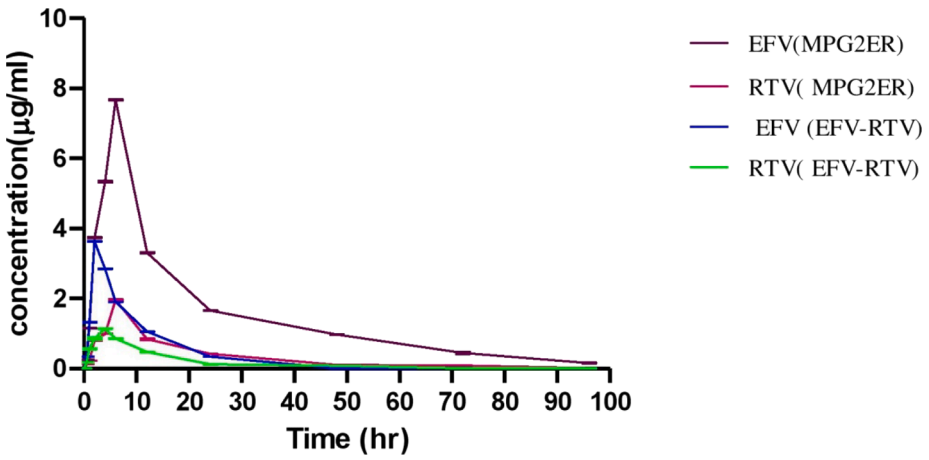

Fig. 11. Comparative plasma concentration of EFV and RTV at different time intervals after administration of MPG2ER by intraperitoneal route (n = 3, Value ± SD).

Table 4a
Pharmacokinetic parameters of EFV in different tissues.

Sr. No	Parameters	Heart	Liver	Spleen	Lymph Node	Kidney	Brain
1	C_{max} (µg/mL)	4.674± 0.025	5.98±0.083	4.576±0.069	3.443±0.048	5.342±0.020	6.653±0.035
2	t_{max} (hr)	6	6	6	6	6	6
3	$t_{1/2}$ (hr)	19.3±0.598	16.89±1.088	21.92±0.250	21±0.054	17.52±0.0127	13.53±0.088
4	MRT (hr)	30.26±1.279	30.72±0.384	32.12±1.653	32.63±0.113	27.31±1.025	26.16±0.284
5	AUC_{tol} (µg/mL)*hr	132.1±1.150	97.88±1.146	88±2.205	96.33±0.190	121.2±0.164	124±1.660
6	AUMC (µg/mL)*hr	4027 ±87.53	2959±32.860	2799±81.109	3143±75.49	3190±6.976	3245±73.69
7	Cl (µg/kg)/((µg/mL)/hr	0.07601±0.003	0.1075±0.008	0.1156±0.002	0.1038±0.002	0.08248±0.001	0.08064±0.001

Note: All values are represented as mean ± SD (n = 3).

Table 4b
Pharmacokinetic parameters of RTV in different tissues.

Sr. No	Parameters	Heart	Liver	Spleen	Lymph Node	Kidney	Brain
1	C_{max} (µg/mL)	2.40±0.015	2.89±0.021	2.13±0.024	2.03±0.042	2.49±0.055	0.79±0.032
2	t_{max} (hr)	4	4	4	4	4	4
3	$t_{1/2}$ (hr)	13.39±0.450	10.88±0.325	13.04±1.025	12.94±1.092	14.66±0.652	6.67±0.792
4	MRT (hr)	15.58±1.925	16.58±0.272	17.97±1.005	16.29±0.937	21.90±0.761	10.53±1.002
5	AUC_{tol} (µg/mL)*hr	18.34±1.190	14.51±2.024	25.82±0.934	25.07±1.305	29.27±1.620	9.25±2.074
6	AUMC (µg/mL)*hr	285.923± 47.303	240.78± 26.201	464.21± 27.094	421.67± 81.067	641.30± 73.625	97.42± 68.213
7	Cl (µg/kg)/((µg/mL)/hr	0.136± 0.032	0.172± 0.012	0.091± 0.043	0.085± 0.007	0.087± 0.036	0.270± 0.008

Note: All values are represented as mean ± SD (n = 3).

determined. To determine the mechanism of drug release, different kinetic models were used. The drug release exponents of EFV and RTV were studied by the Korsmeyer–Peppas equation (Nguyen et al, 2022; Zaman et al, 2022), and the regression coefficients (R^2) were calculated, as shown in Tables 1(a) and 1(b). At both pH (7.4 and 4), the EFV and RTV released from MPG2ER followed Higuchi release, with correlation coefficients greater than zero. This suggests that the EFV and RTV released from the MPG2ER at pH 7.4 and 4 followed the square root of the diffusion mechanism in a time-dependent manner. This mechanism followed an initial burst release during the initial 12 hrs when the concentrations of encapsulated EFV and RTV were high. This was followed by gradual and continuous release of the drug for up to 96 hrs (Patri et al, 2005). According to data from the Korsmeyer-Peppas release exponent, MPG2ER showed a non-fiction anomalous release with an n value greater than 0.5 and less than 1. It is caused by typical diffusion and matrix erosion (Shah & Khan, 2012).

4.4. *In vitro ligand agglutination assay*

PG2 surfaces functionalized with d-mannose dendrimers were synthesized to target the DC-SIGN receptor on dendritic cells and were evaluated by a concanavalin A (ConA) enzyme-linked assay. The optical density was measured at 550 nm after the addition of 10 % MPG2ER with different concentrations of Con A. The optical density gradually increased with increasing Con A concentration and duration of exposure, as shown in Fig. 6. The optical density did not significantly ($p > 0.05$) increase after 500 µg/ml. Therefore, there was no change in optical density after 120 min ($p > 0.05$), which indicates that the binding site of Con A was saturated.

4.5. *Cell viability assay*

The cellular toxicity of MPG2ER was determined by using an MTT assay with the immune H9 cell line. Cell viability was monitored by determining intracellular ATP levels after treatment of cells with 5-fluorouracil (5-FU), EFV-RTV, MPG2 or MPG2ER.

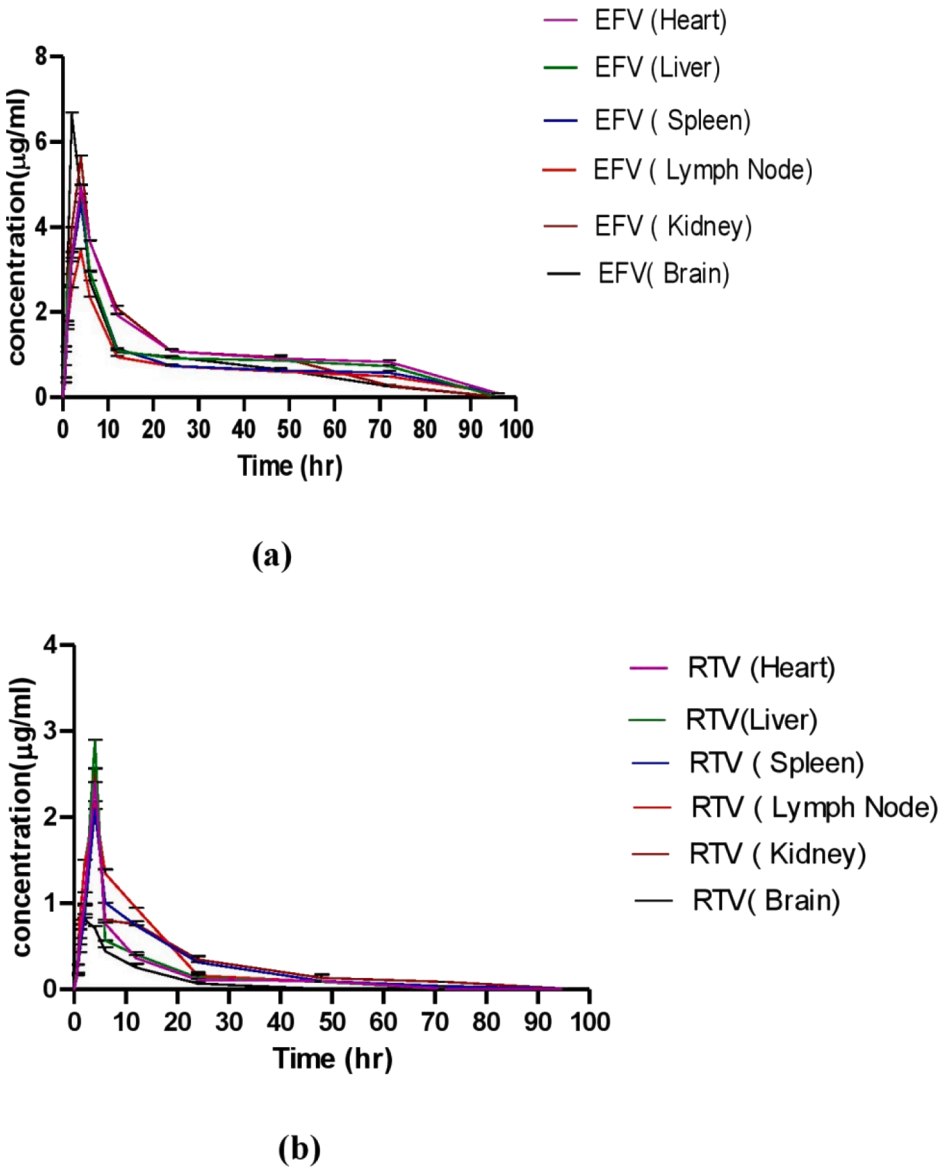

Fig. 12. The concentration of EFV (a) and RTV(b) in different tissue after treatment of MPG2ER.

EFV-RTV was safe at concentrations up to 12.5 µg/ml, while the IC_{50} was 59.48 µg/ml, as shown in Fig. 7 **(a)**. The IC_{50} value of PG2 was 42.79 µg/ml, which improved to 75 %. The concentrations of MPG2ER were 94 µg/ml and 76.27 µg/ml, as shown in Table 2. The number of surviving cells was lower in the PG2 group (Fig. 7(b)**),** and the cells exhibited aggregation and numerous abnormally sized nuclei, which indicated cytotoxicity, as indicated in Fig. 7(c)**.** The cationic surface charge of PG2 has been shown to interact with the negatively charged cell membrane and cause cytotoxicity(Janaszewska et al, 2019), which is neutralized by mannosylation and greatly improves cell viability, as depicted in Fig. 7 **(d) and (e)**.

4.6. Confocal microscopy

The cellular uptake of fluorescently tagged EFV-RTV and MPG2ER was qualitatively assessed by confocal analysis and quantitatively assessed by flow cytometry. Acridine orange (AO) and EtBr dyes have *meta*-chromic characteristics that are frequently used to assess the physiology of the cell and the status of the cell cycle. AO is an intercalating dye that produces green luminescence by binding nucleic acids (DNA or RNA) in all nucleated cells (live cells). This binding was a result of the interaction of AO molecules and nucleic acid base pairs. However, EtBr was used for the identification of dead cells and for the detection of green fluorescence (Ashraf et al, 2017).

Treatment with EFV-RTV and MPG2ER induced significant morphological alterations in H9 cell apoptosis. However, morphological alterations were observed in MPG2ER treated cells, as shown in Fig. 8 (MPG2ER merged). Compared to those of the EFV-RTV group, the EFV-RTV group displayed more intense green nuclei as a result of drug uptake. Nevertheless, H9 cells treated with EFV-RTV produced a few green puncta, as shown in Fig. 8 (EFV-RTV merged). Therefore, it was confirmed that the MPG2ER was uniformly distributed in H9 cells with less cytotoxicity.

4.7. Flow cytometry

Flow cytometry was used to assess apoptosis and drug uptake by counting the number of cells that were internalized due to fluorescence-labeled MPG2ER. In this study, we compared the drug uptake of EFV-RTV by H9 cells with that of the MPG2ER nanoformulation at a concentration of 10 µM/ml.

Apoptotic cascades bear significant purposes in HIV pathogenesis

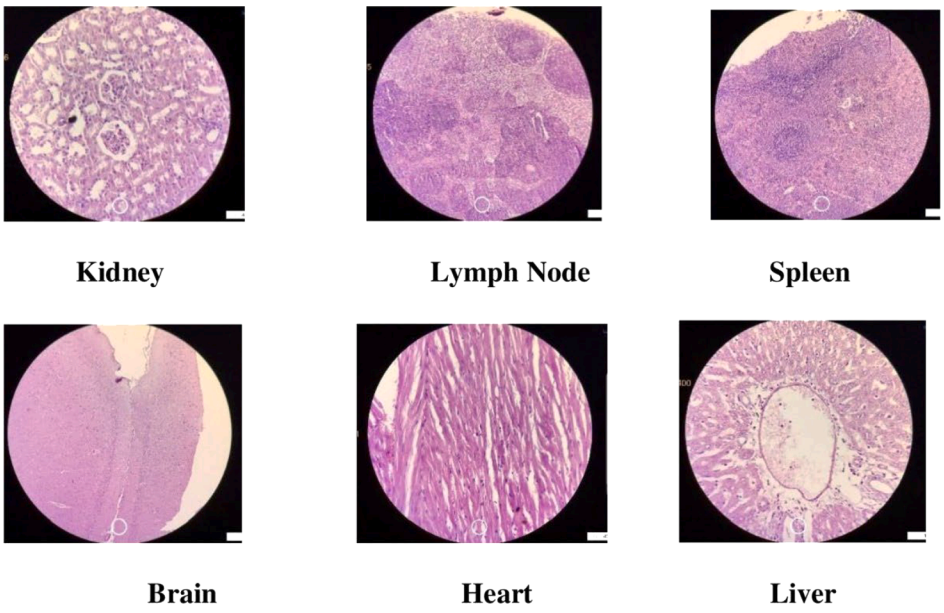

Fig. 13. Light microscope images of the heart, liver, spleen, lymph node, kidney, and brain tissue with hematoxylin and eosin stain illustrated the histopathological impacts after intraperitoneal administration of MPG2ER at a dose level 10 mg/kg after 12 hrs.

Table 5
Different parameters of MPG2ER when stored under various conditions of temperature (0∘C, Room Temperature, and 60∘C) after keeping in dark and light.

Parameter	Ambered color vials			Colorless vials		
	0 °C	Room temp	60 °C	0 °C	Room temp	60 °C
Color	Cream color	Cream color	Light brown	Cream color	Cream color	Light brown
Flow	Free flow	Free flow	Sticky	Free flow	Sticky	Sticky
% drug content of EFV	89.132	88.126	79.422	86.311	76.190	63.022
% drug content of RTV	87.065	82.243	75.152	80.318	70.622	52.136
% hemolysis	4.196	4.275	5.324	4.161	4.405	9.862

and progressions. In HIV infections, viral proteins bind to the TNFR and exhibit both pro- and anti-apoptotic properties (Jabea Ekabe et al, 2022). EFV-RTV and MPG2ER were added at a concentration of 10 μM, followed by counting of early and late apoptotic cells; using Annexin V-FITC and PI dyes. The fluorescence label Annexin V-FITC follows the internalization of EFV-RTV and MG2ER in live H9 cells. However, PI is a nuclear stain dye that only enters after the loss of cell membrane integrity. Therefore, PI staining predicted H9 cell viability. In negative control H9 cells, 0.2 % of the cells were Annexin V-FITC (+)/PI (+). However, 25.2 % and 32.2 % of the EFV-RTV- and MPG2ER-treated cells, respectively, were Annexin V-FITC (+)/PI(+) and showed late apoptosis. However, 15.3 % and 19.56 % of the EFV-RTV- and MPG2ER-treated cells, respectively, were Annexin V-FITC (+)/PI (−), indicating early apoptosis.

Typical double scatter FSC-SSC plots with the fluorescence intensity of cells were determined by exposing the fluorescently labeled EFV-RTV and MPG2ER, as depicted in Fig. 9 **(f) and (i),** respectively**.** The double scatter plots of side scattering (SSC linear) against forward scattering (FSC linear) of untreated cells and cells exposed to 10 μM/ml EFV-RTV and MPG2ER for 24 hrs are shown in Fig. 9 **(e) and (h)**. Both the internal complexity and size of untreated H9 cells were not altered, as measured by SSC and FSC, as shown in Fig. 9 **(c)**. On the other hand, EFV and RTV uptake within the cells was affected by the administration of MPG2ER and EFV-RTV, which impacted SSC distribution.

In contrast to treatment with EFV-RTV, treatment with MPG2ER significantly increased the extent of SSC distribution, which was internalized by living cells (Fig. 9 **(e)**). The internal complexity increased after MPG2ER therapy. Treatment with MPG2ER increased the intensity of side scattering, which confirmed the increased EFV and RTV uptake. An increase in the intensity of SSC distribution with respect to Annexin-V-FITC followed by treatment with MPG2ER showed internalization of EFV and RTV in cells without compromising the integrity of the plasma membrane, as shown in Fig. 9 **(g)**. It promoted late apoptosis and assisted in removing necrotic cells. These findings confirmed that MPG2ER effectively decreases the viral load in the treatment of HIV. Cells present outside the circle denoted cell debris and showed minimum light scattering, as shown in Fig. 9 **(f).** A typical flow cytometry histogram was used to quantitatively determine drug uptake after H9 cells were exposed to EFV-RTV and MPG2ER, as shown in Fig. 10. Compared to that of EFV-RTV, the drug uptake by MPG2ER was 81.2 %, which was significantly greater, as shown in Fig. 10 **(b) and (c)**. We also reported that distribution of cell fluorescence shifted to greater values for MPG2ER-treated cells than for EFV-RTV-treated cells. It was concluded that cells take up MPG2ER more effectively.

4.8. Pharmacokinetic study

A single 10 mg/kg equivalent dose of EFV-RTV and MPG2ER was administered intraperitoneally to male Wistar rats to estimate the plasma concentrations of EFV and RTV by non-compartmental analysis. The relative bioavailability of MPG2ER was determined by assessing the total area under the curve (AUC) with respect to free EFV-RTV. Subsequently, other pharmacokinetic parameters, including the half-life and clearance, were also calculated and are reported in Tables 3(a) and 3(b).

The results showed that delivery of the MPG2ER nanoformulation potentially improved the relative bioavailability of EFV and RTV. The ultimate biodistribution and blood clearance of PAMAM dendrimers are influenced by surface charge and particle size. Therefore, the nanosized

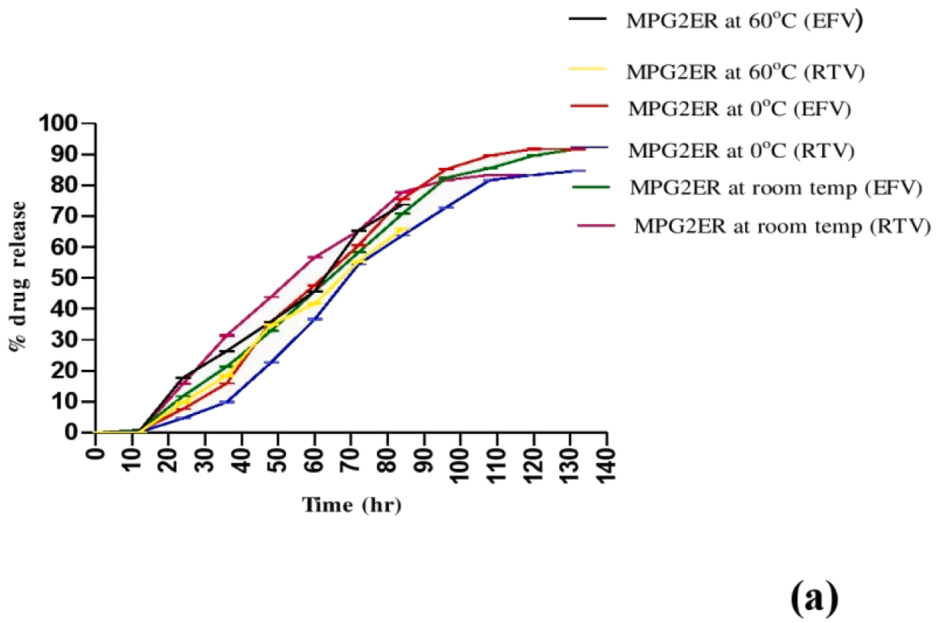

Fig. 14. Percentage of EFV and RTV release at pH 7.4 after storage in ambered color (a), colorless vial (b) and different temperature condition.

Table 6a
Release kinetics of EFV and RTV from MPG2ER under various conditions of temperature (0∘C, Room Temperature and 60∘C) after keeping in dark.

Formulation	Temp	Zero Order(R^2)	First Order(R^2)	Higuchi Model(R^2)	Korsmeyes-Peppas Model(R^2)	EFV release exponent (n)
RTV(MPG2ER)	0 °C	0.861	0.967	0.976	0.958	0.587
RTV(MPG2ER)	Room temp	0.869	0.926	0.983	0.924	0.617
RTV(MPG2ER)	60 °C	0.901	0.961	0.974	0.963	0.617
EFV(MPG2ER)	0 °C	0.891	0.967	0.986	0.968	0.619
EFV(MPG2ER)	Room temp	0.925	0.980	0.984	0.968	0.615
EFV(MPG2ER)	60 °C	0.893	0.966	0.986	0.958	0.597

Table 6b
Release kinetics of EFV and RTV from MPG2ER under various conditions of temperature (0∘C, Room Temperature and 60∘C) after keeping in light.

Formulation	Temp	Zero Order(R^2)	First Order(R^2)	Higuchi Model(R^2)	Korsmeyes-Peppas Model(R^2)	EFV release exponent (n)
RTV(MPG2ER)	0 °C	0.861	0.967	0.978	0.928	0.58
RTV(MPG2ER)	Room temp	0.893	0.972	0.994	0.957	0.61
RTV(MPG2ER)	60 °C	0.891	0.986	0.957	0.925	0.64
EFV(MPG2ER)	0 °C	0.891	0.988	0.991	0.967	0.57
EFV(MPG2ER)	Room temp	0.954	0.970	0.989	0.958	0.59
EFV(MPG2ER)	60 °C	0.902	0.987	0.975	0.941	0.62

and combined charge of MPG2 improved the pharmacokinetic behavior of EFV and RTV through sustained release for up to 96 hrs and 72 hrs, respectively, as shown in Fig. 11. According to the literature, dendrimers are particularly taken up through enterocytes and gut-associated lymphoid tissue. After that, the drug was released slowly, and the circulation was prolonged. The aforementioned findings supported this mechanism to enhance MRT and AUC_{tol} up to 3 times, which ultimately increased the bioavailability of EFV and RTV (Aji Alex et al, 2011). Compared with those of EFV-RTV, the C_{max} (7.68 ± 0.121 μg/mL) and $t_{1/2}$ (19.09 ± 0.890 hrs) of EFV significantly increased through the MPG2ER, as indicated by improved absorption and blood circulation time. The absorption of MPG2ER was confirmed to bypass the encapsulated drug from gastric and intestinal degradation. Subsequently, the possible uptake and transport of MPG2ER through the intestinal mucosa were confirmed. (Oddone et al, 2016). The bio-adhesive properties of PG2 were also enhanced by conjugation with d-mannose, which also protects the surface of dendrimers from aggregation, opsonization, and phagocytosis (Ogunwuyi et al, 2016).

4.9. Tissue distribution study

The tissue distribution study revealed that all pharmacokinetic parameters, such as MRT, t_{max}, C_{max}, $t_{1/2}$, and $AUC_{tol,}$ for EFV and RTV through MPG2ER were approximately 2 times greater in all tissues than in plasma, as shown in Tables 4(a) and 4(b). This result suggested that compared with free EFV-RTV, EFV and RTV released through the MPG2ER were bound to the target tissue (Kharwade et al, 2022). MPG2ER specifically influenced the EFV and RTV distribution in the lymph node and spleen. Therefore, MPG2ER could be a useful strategy for eradicating HIV infection from viral reservoir tissue. Thus, the use of MPG2 dendrimers is an attractive approach for increasing the therapeutic efficacy of this drug.

According to the literature, PAMAM dendrimers cannot be excreted through the renal system. Additionally, the mannosylation of PG2 decreases the clearance of MPG2ER and increases the MRT and $t_{1/2}$. However, opsonization is necessary for their absorption and biodistribution. Thus, MPG2 is easily sequestered in the liver. The tissue distribution of EFV from the MPG2ER among different organs decreased in the following order: brain > liver > heart > spleen > lymph node > kidney, as shown in Fig. 12. Above, tissue distribution data, adopting such novel approach was further favoring promising roles of MPG2ER to limit their unwanted tissue distribution and blood viremia levels with minimal reported toxicity events.

4.10. Histopathology study

All of the abovementioned organ tissues were observed for complete microscopic analysis and determination of tissue toxicity. Hydrated 7 μm thick paraffin sections of each tissue sample were examined under a light microscope, as shown in Fig. 13.

Interestingly, almost all tissues treated with MPG2ER showed no signs of cytotoxicity. Liver sections revealed a distinctive hepatic portal vein with binucleated cells; decreased kupffer cells activation events as well as tubular cell hyalinization incidences. However, some cases of very mild peritubular edema but without any sign of irritation were also observed, in some parts of liver tissue. Granular leukocytes were found between lymphocytes as well as giant macrophages in the spleen segment, which also revealed healthy lymphoid follicles that were encircled by these cells. The ectatic medullary sinus was not present in the lymph node, but there was a small expansion of the marginal zone. The kidney and heart did not exhibit any unusual alterations. No cytological alterations were observed in the whole-mount tissue. However, light microscopic analysis of the brain after MPG2ER treatment revealed large to medium-sized blood vessels, with hyalinization. Whereas open-faced oval nuclei with prominent nucleoli were reported with neuronal cells.

4.11. Stability studies

The stability of MPG2ER was studied at different temperatures (0 °C, room temperature 27 °C, and 60 °C) after it was stored in the dark (in amber-colored vials) or light (in colorless vials). The results showed that after 6 weeks, the MPG2ER was less stable at an accelerated temperature (60 ± 2 °C) in the light. Under these conditions, the mixture was sticky and dark because of the acceleration of polymerization.

It was most stable at low temperatures (0 °C) and at room temperature in the dark. There was no change in the color or flow properties, and no hemolysis was detected at low temperatures (0 °C) or at room temperature in the dark, as shown in Table 5. However, the formulation showed hemolysis and decreased the % drug content and flow in colorless vials at low temperatures (0 °C) as well as at room temperature, as shown in Table 5. So, the currently synthesized dendrimer-based systems may be stable at room temperature, maintained in the dark.

The percent drug release was found to be fast at 60 ± 2 °C in the dark as well as in the light. At higher temperatures, the loss of drug was greater in the presence of light, as shown in Fig. 14 **(a) and (b).** The EFV and RTV release from MPG2ER followed Higuchi release kinetics with a non-Fickian release exponent at 0 °C and at room temperature, as shown in Table 6(a) and 6(b). However, when stored in light at 60 ± 2 °C, first-order release kinetics followed, which showed drastically decreased stability.

5. Discussion

Disease management in HIV infection patients is challenging due to the very limited accessibility of administered ART drugs towards latent viral reservoirs. Various factors, including viral reservoirs, poor organ perfusion, low bioavailability, severe side effects, and drug resistance, make HIV treatment challenging (Kharwade et al, 2020a; Chen et al, 2022). Thus, the MPG2ER has been shown to target viral reservoir tissue (lymph nodes and spleen) and regulate the release rate.

PAMAM G2, which is encoded by carbohydrates focused on d-mannose, is beneficial for DC-SIGN binding (Albertazzi et al, 2013) as well as decreasing cytotoxicity. Therefore, d-mannose was used to functionalize the peripheral cationic group of PG2. Mannosylation significantly increased cell survival by neutralizing the peripheral cationic charge on PG2 (Owens & Peppas, 2006; Kharwade et al, 2021). The intrinsic properties of MPG2 dendrimers are determined by their high entrapment efficiency and loading capacity (Shadrack et al, 2018). An in vitro ligand agglutination assay revealed the affinity of DC-SIGN

for the receptor of dendritic cells. Therefore, mannosylation strongly blocked the interaction between gp120 in HIV and dendritic cells (Kawakami et al, 2000). A flow cytometry study revealed that MPG2ER strongly increased drug uptake (Kolhatkar et al, 2007). Confocal microscopy also confirmed that MG2ER had more bright green nuclei than free EFV-RTV, which showed significant drug accumulation in cells. This was due to drug uptake with condensation and fragmentation of chromatin in the nucleus and significantly increased apoptosis (Sadekar & Ghandehari, 2012).

A greater lymphatic therapeutic index of the drug is expected in patients with lymph-resistant diseases. However, for lymph targeting, the drug carrier must such a small dimensions which would ensure their entries into lymphatic tissue (such as the spleen and lymph nodes) and large enough to be retained (Kharwade et al, 2020b; Akkewar et al, 2022). The physical dimension of the synthesized MPG2ER (7–10 nm) was smaller than that of typical proteins. It also assisted in reducing diffusion layer the thickness and increasing the rate of dissolution (Horter & Dressman, 1997). As a result, the bioavailability and tissue retention intervals of the loads through MPG2ER increased 3-fold with respect to those of free EFV-RTV. The histopathological analysis revealed no cell impairment or tissue toxicity after the treatment with MPG2ER. Hence, it was concluded that the MPG2ER were biocompatible and efficacious formulation.

From the drug release study, it was observed that compared with PBS, MPG2ER released more of both drugs at an acetate pH. This was possibly due to the amino and partial carbohydrate groups present on the surface of the PAMAM dendrimers. These groups support protonation, repelling, and transport through a conformational change in the MPG2ER at acidic pH and facilitate the release of EFV and RTV once the formulation penetrates HIV-infected cells (Lee, JH., Yeo, 2016). Therefore, it was concluded that such prolonged and controlled drug release were dependent on the facts of partitioning of the loads into the core of MPG2 and peripheral quaternary ammonium ions with carbohydrate moieties.

Stability study reported photostability issues of MPG2ER at elevated temperatures. Marin et al, (2013) had reported that at elevated temperature, the free energy level and chemical kinetics are proportionally increased, which lead to adversely affected uniform ring-like structures of the dendrimers and led them to get destabilized, resulting in pre-release of the loads (Marin et al, 2013). Whereas, at 0 °C storage temperature; there was no change in the release profile of the drug from the MPG2ER. Based on a literature survey, we hypothesized that at such a low temperature, there was of significant reduction in energy levels which leads to a decreased in overall available energy, required for efficient interactions with drug molecules. Hence, such events leads to some hypothetical shrinking of the dendritic structures and geometry in three-dimensional space (Mhlwatika & Aderibigbe, 2018). Therefore, it was confirmed that the efficacy of MPG2ER should preferably be stored at 0 °C, in the dark.

HIV infections are typically described in terms of the distinguished viral proteins presences; may essentially bearing pro-apoptotic and anti-apoptotic attributes. PAMAM helps to inhibit the binding of TAT protein to TAR RNA of HIV and diminishes HIV transcription. Subsequently, the mannosylation of PG2 potentially targets HIV-infected dendritic cells and decreases the viral load by increasing apoptosis (Ahr et al, 2004). The flow cytometry results showed that compared with free EFV-RTV, MPG2ER induced both early and late apoptosis. As early apoptosis increases, the MPG2ER influences drug uptake by inducing HIV-1 GagPol dimerization in productively infected cells, and late apoptosis has been shown to reduce the number of HIV-1-interacting cells. Therefore, MPG2ER has therapeutic potential in HIV treatment via increased cell apoptosis, resulting in clinical improvement (Herbeuval et al, 2005).

6. Conclusion

Dendritic cells are one of the targets and entry sites of HIV. Therefore, dendritic cells of the infected lymph node and spleen are considered a viral reservoir for spreading HIV. The use of mannosylated PG2 dendrimers is considered the backbone for effectively targeting the HIV viral reservoir. For this purpose, dual-loaded EFV with a booster RTV, within MPG2 dendrimers, were successfully synthesized, characterized and evaluated. The above formulation showed sustained release and an acid-sensitive drug release mechanism, which facilitated its release in HIV-infected cells. The formulation showed less cytotoxicity with enhanced drug uptake compared to free EFV-RTV. An in vitro ligand agglutination study revealed that MPG2ER has a potent binding affinity for the DC-SIGN receptor. Confocal and flow cytometry studies revealed that EFV and RTV were effectively internalized by H9 cells via the MPG2ER. It also increased late apoptosis, which contributed to a significant lowering in the infected cell counts and viral loads. MPG2ER offers a unique formulation approach for potentially enhancing the bioavailability of EFV. It also revealed greater spleen and lymph node accumulation with no tissue toxicity. Therefore, the above study potentially favor promising MPG2ER roles and their clinical scope as a biocompatible novel drug carrier to reduce the viral load in major HIV reservoir tissues with targeted efficacies and improved bioavailability.

Author contributions

All authors have accepted responsibility for the entire content of this manuscript and approved its submission.

Funding information

The authors would like to extend their sincere ‘appreciation to the Researchers Supporting Project Number (RSP2024R301), King Saud University, Riyadh, Saudi Arabia.

CRediT authorship contribution statement

Rohini Kharwade: Writing – original draft, Methodology, Investigation, Formal analysis, Data curation, Conceptualization. **Mohsin Kazi:** Writing – review & editing, Validation, Resources, Funding acquisition, Formal analysis. **Nilesh Mahajan:** Writing – review & editing, Project administration, Investigation, Conceptualization. **Payal Badole:** Writing – review & editing. **Sachin More:** Writing – review & editing, Validation, Software, Investigation. **Asaad Kayali:** Writing – review & editing. **Md Noushad Javed:** Writing – review & editing, Visualization, Conceptualization. **Mohammed Kaleem:** Writing – review & editing, Writing – original draft, Validation, Methodology.

Declaration of competing interest

The authors declare that they have no known competing financial interests or personal relationships that could have appeared to influence the work reported in this paper.

Data availability

Data will be made available on request.

Acknowledgment

The authors would like to extend their sincere appreciation to the Researchers Supporting Project Number (RSP2024R301), King Saud University, Riyadh, Saudi Arabia. Authors would like to acknowledge the Dadasaheb Balpande College of Pharmacy, Rashtrasant Tukadoji Maharaj Nagpur University, Nagpur, (MS)–440037, India, for providing the necessary infrastructure to conduct the experimental work.

References

Ahr B, Robert-hebmann V, Devaux C, Biard-piechaczyk M (2004) Apoptosis of uninfected cells induced by HIV envelope glycoproteins. **12**: 1–12, doi:10.1186/1742-4690-1-12.

Aji Alex, M.R., Chacko, A.J., Jose, S., Souto, E.B., 2011. Lopinavir loaded solid lipid nanoparticles (SLN) for intestinal lymphatic targeting. Eur. J. Pharm. Sci. 42, 11–18. https://doi.org/10.1016/j.ejps.2010.10.002.

Akkewar, A., Mahajan, N., Kharwade, R., Gangane, P., 2022. Liposomes in the Targeted Gene Therapy of Cancer: A Critical Review. Curr. Drug Deliv. 20, 350–370. https://doi.org/10.2174/1567201819666220421113127.

Albertazzi, L., Gherardini, L., Brondi, M., Sulis Sato, S., Bifone, A., Pizzorusso, T., Ratto, G.M., Bardi, G., 2013. In vivo distribution and toxicity of PAMAM dendrimers in the central nervous system depend on their surface chemistry. Mol. Pharm. 10, 249–260. https://doi.org/10.1021/mp300391v.

Alghamdi, R.M., Hassan, M.A., Kaleem, M., Kayali, A., Halwani, M.A., Zamzami, M.A., Choudhry, H., Alhosin, M., 2020. Targeting Itch/p73 pathway by thymoquinone as a novel therapeutic strategy for cancers with p53 mutation. Eur J Cell Sci 2, 20–26. https://doi.org/10.34154/2020-ejcs-0201-20-26/euraass.

Ashraf, W., Bronner, C., Zaayter, L., Ahmad, T., Richert, L., Alhosin, M., Ibrahim, A., Hamiche, A., Mely, Y., Mousli, M., 2017. Interaction of the epigenetic integrator UHRF1 with the MYST domain of TIP60 inside the cell. J. Exp. Clin. Cancer Res. 36, 188. https://doi.org/10.1186/s13046-017-0659-1.

Chaubey, P., Mishra, B., 2014. Mannose-conjugated chitosan nanoparticles loaded with rifampicin for the treatment of visceral leishmaniasis. Carbohydr. Polym. 101, 1101–1108. https://doi.org/10.1016/j.carbpol.2013.10.044.

Chen, J., Zhou, T., Zhang, Y., Luo, S., Chen, H., Chen, D., Li, C., Li, W., 2022. The reservoir of latent HIV. Front. Cell. Infect. Microbiol. 12 https://doi.org/10.3389/fcimb.2022.945956.

Dutta, T., Jain, N.K., 2007. Targeting potential and anti-HIV activity of lamivudine loaded mannosylated poly (propyleneimine) dendrimer. Biochim Biophys Acta - Gen Subj 1770, 681–686. https://doi.org/10.1016/j.bbagen.2006.12.007.

Filipczak, N., Yalamarty, S.S.K., Li, X., Parveen, F., Torchilin, V., 2021. Developments in treatment methodologies using dendrimers for infectious diseases. Molecules 26. https://doi.org/10.3390/molecules26113304.

Fule, R., Kaleem, M., Asar, T.O., Rashid, M.A., Shaik, R.A., Eid, B.G., Nasrullah, M.Z., Ahmad, A., Kazmi, I., 2023. Formulation, optimization and evaluation of cytarabine-loaded iron oxide nanoparticles: from in vitro to in vivo evaluation of anticancer activity. Nanomaterials 13. https://doi.org/10.3390/nano13010175.

Heidegger S, Gößl D, Schmidt A, Niedermayer S, Argyo C, Endres S, Bein T, Bourquin C (2015) silica nanoparticles for targeted drug delivery †. doi:10.1039/c5nr06122a.

Herbeuval J, Boasso A, Grivel J, Hardy AW, Anderson SA, Dolan MJ, Chougnet C, Lifson JD, Shearer GM (2005) TNF-related apoptosis-inducing ligand (TRAIL) in HIV-1 – infected patients and its in vitro production by antigen-presenting cells. **105**: 2458–2464, doi:10.1182/blood-2004-08-3058.Supported.

Horter, D., Dressman, J.B., 1997. Influence of physicochemical properties on dissolution of drugs in the gastrointestinal tract. Adv. Drug Deliv. Rev. 25, 3–14. https://doi.org/10.1016/S0169-409X(96)00487-5.

Hull, M.W., Montaner, J.S.G., 2011. Ritonavir-boosted protease inhibitors in HIV therapy. Ann. Med. 43, 375–388. https://doi.org/10.3109/07853890.2011.572905.

Iannazzo D, Pistone A, Romeo R, Sv G (2015) Nanotechnology Approaches for Antiretroviral Drugs Delivery. **1**: 1–13, doi:10.15744/2454-499X.1.201.

Jabea Ekabe, C., Asaba Clinton, N., Agyei, E.K., Kehbila, J., 2022. Role of apoptosis in HIV pathogenesis. Adv Virol 2022. https://doi.org/10.1155/2022/8148119.

Jain, K., Kesharwani, P., Gupta, U., Jain, N.K., 2010. Dendrimer toxicity: let's meet the challenge. Int. J. Pharm. 394, 122–142. https://doi.org/10.1016/j.ijpharm.2010.04.027.

Janaszewska, A., Lazniewska, J., Trzepiński, P., Marcinkowska, M., Klajnert-Maculewicz, B., 2019. Cytotoxicity of dendrimers. Biomolecules 9. https://doi.org/10.3390/biom9080330.

Jin, W., Li, C., Du, T., Hu, K., Huang, X., Hu, Q., 2014. DC-SIGN plays a stronger role than DCIR in mediating HIV-1 capture and transfer. Virology 458–459. https://doi.org/10.1016/j.virol.2014.04.016.

Kaleem M, Kayali A, Sheikh RA, Kuerban A, Hassan MA, Almalki NAR, Al-abbasi FA, Anwar F, Omran Z, Alhosin M (2024) In Vitro and In Vivo Preventive Effects of Thymoquinone against Breast Cancer : Role of DNMT1. **996**:.

Kappelhoff, B.S., Crommentuyn, K.M.L., De Maat, M.M.R., Mulder, J.W., Huitema, A.D. R., Beijnen, J.H., 2004. Practical guidelines to interpret plasma concentrations of antiretroviral drugs. Clin. Pharmacokinet. 43, 845–853. https://doi.org/10.2165/00003088-200443130-00002.

Kawakami, S., Sato, A., Nishikawa, M., Yamashita, F., Hashida, M., 2000. Mannose receptor-mediated gene transfer into macrophages using novel mannosylated cationic liposomes. Gene Ther. 7, 292–299. https://doi.org/10.1038/sj.gt.3301089.

Kharwade, R., More, S., Mahajan, N., Agrawal, P., 2020a. functionalised dendrimers: potential tool for antiretroviral therapy. Curr. Nanosci. 16, 708–722. https://doi.org/10.2174/1573413716666200213114836.

Kharwade, R., More, S., Warokar, A., Agrawal, P., Mahajan, N., 2020b. Starburst pamam dendrimers: Synthetic approaches, surface modifications, and biomedical applications. Arab. J. Chem. 13, 6009–6039. https://doi.org/10.1016/j.arabjc.2020.05.002.

Kharwade, R., Badole, P., Mahajan, N., More, S., 2021. Toxicity and surface modification of dendrimers: a critical review. Curr. Drug Deliv. 18, 1–15. https://doi.org/10.2174/1567201818666211021160441.

Kharwade, R., More, S., Suresh, E., Warokar, A., Mahajan, N., 2022. Improvement in bioavailability and pharmacokinetic characteristics of efavirenz with booster dose of ritonavir in PEGylated PAMAM G4 dendrimers. AAPS PharmSciTech. https://doi.org/10.1208/s12249-022-02315-8.

Kharwade, R., Mahajan, N., More, S., Warokar, A., Dhobley, A., Palve, D., 2023. Effect of PEGylation on drug uptake, biodistribution, and tissue toxicity of efavirenz – ritonavir loaded PAMAM G4 dendrimers. Pharm. Dev. Technol. 1–19. https://doi.org/10.1080/10837450.2023.2173230.

Kolhatkar, R.B., Kitchens, K.M., Swaan, P.W., Ghandehari, H., 2007. Surface acetylation of polyamidoamine (PAMAM) dendrimers decreases cytotoxicity while maintaining membrane permeability. Bioconjug. Chem. 18, 2054–2060. https://doi.org/10.1021/bc0603889.

Lee, J.H., Yeo, Y., 2016. Controlled drug release from pharmaceutical nanocarriers jinhyun. Chem. Eng. Sci. 24, 75–84. https://doi.org/10.1016/j.ces.2014.08.046.Controlled.

Makwana, V., Jain, R., Patel, K., Nivsarkar, M., Joshi, A., 2015. Solid lipid nanoparticles (SLN) of Efavirenz as lymph targeting drug delivery system: elucidation of mechanism of uptake using chylomicron flow blocking approach. Int. J. Pharm. 495, 439–446. https://doi.org/10.1016/j.ijpharm.2015.09.014.

Marin, E., Briceño, M.I., Caballero-George, C., 2013. Critical evaluation of biodegradable polymers used in nanodrugs. Int. J. Nanomed. 8, 3071–3091. https://doi.org/10.2147/IJN.S47186.

Mhlwatika, Z., Aderibigbe, B.A., 2018. Application of dendrimers for the treatment of infectious diseases. Molecules 23. https://doi.org/10.3390/molecules23092205.

Michniak-Kohn BB, Deol PK, Kotta S, Aldawsari HM, Badr-Eldin SM, Nair AB, Kaleem M, Dalhat MH (2022) Thermosensitive Hydrogels Loaded with Resveratrol Nanoemulsion: Formulation Optimization by Central Composite Design and Evaluation in MCF-7 Human Breast Cancer Cell Lines. doi:10.3390/gels8070450.

Nelson, A.G., Zhang, X., Ganapathi, U., Szekely, Z., Flexner, C.W., Owen, A., Sinko, P.J., 2015. Drug delivery strategies and systems for HIV/AIDS pre-exposure prophylaxis and treatment. J. Control. Release 219, 669–680. https://doi.org/10.1016/j.jconrel.2015.08.042.

Nguyen, T.T., Nguyen, B.P., Nguyen, D.T.D., Nguyen, N.H., Nguyen, D.H., Nguyen, C.K., 2022. Retrovirus drugs-loaded PEGylated PAMAM for prolonging drug release and enhancing efficiency in HIV treatment. Polymers (basel) 14. https://doi.org/10.3390/polym14010114.

Oddone, N., Lecot, N., Fernández, M., Rodriguez-Haralambides, A., Cabral, P., Cerecetto, H., Benech, J.C., 2016. In vitro and in vivo uptake studies of PAMAM G4.5 dendrimers in breast cancer. J. Nanobiotechnol. 14, 1–12. https://doi.org/10.1186/s12951-016-0197-6.

Ogunwuyi, O., Kumari, N., Smith, K.A., Bolshakov, O., Adesina, S., Gugssa, A., Anderson, W.A., Nekhai, S., Akala, E.O., 2016. Antiretroviral Drugs-Loaded Nanoparticles Fabricated by Dispersion Polymerization with Potential for HIV/AIDS Treatment. Infect. Dis. Res. Treat 9. https://doi.org/10.4137/idrt.s38108. IDRT. S38108.

Owens, D.E., Peppas, N.A., 2006. Opsonization, biodistribution, and pharmacokinetics of polymeric nanoparticles. Int. J. Pharm. 307, 93–102. https://doi.org/10.1016/j.ijpharm.2005.10.010.

Park J, Ha MK, Yang N, Yoon TH (2017) Flow cytometry – based quantification of cellular Au nanoparticles. doi:10.1021/acs.analchem.6b04418.

Patri, A.K., Kukowska-Latallo, J.F., Baker, J.R., 2005. Targeted drug delivery with dendrimers: Comparison of the release kinetics of covalently conjugated drug and non-covalent drug inclusion complex. Adv. Drug Deliv. Rev. 57, 2203–2214. https://doi.org/10.1016/j.addr.2005.09.014.

Pau, A.K., George, J.M., 2014. Antiretroviral therapy: current drugs. Infect. Dis. Clin. North Am. 28 https://doi.org/10.1016/j.idc.2014.06.001.

Peng J, Wu Z, Qi X, Chen Y, Li X (2013) Dendrimers as potential therapeutic tools in HIV inhibition.

Pyreddy, S., Kumar, P., Kumar, P., 2014. Polyethylene glycolated PAMAM dendrimers-Efavirenz conjugates. Int. J. Pharm. Investig. 4, 15. https://doi.org/10.4103/2230-973x.127735.

Rojekar, S., Fotooh Abadi, L., Pai, R., Mahajan, K., Kulkarni, S., Vavia, P.R., 2021a. Multi-organ targeting of HIV-1 viral reservoirs with etravirine loaded nanostructured lipid carrier: An in-vivo proof of concept. Eur. J. Pharm. Sci. 164, 105916 https://doi.org/10.1016/j.ejps.2021.105916.

Rojekar, S., Pai, R., Abadi, L.F., Mahajan, K., Prajapati, M.K., Kulkarni, S., Vavia, P., 2021b. Dual loaded nanostructured lipid carrier of nano-selenium and Etravirine as a potential anti-HIV therapy. Int. J. Pharm. 607, 120986 https://doi.org/10.1016/j.ijpharm.2021.120986.

Sadekar, S., Ghandehari, H., 2012. Transepithelial transport and toxicity of PAMAM dendrimers: Implications for oral drug delivery. Adv. Drug Deliv. Rev. 64, 571–588. https://doi.org/10.1016/j.addr.2011.09.010.

Seitz, R., 2016. Human immunodeficiency virus (HIV). Transfus Med. Hemotherapy 43. https://doi.org/10.1159/000445852.

Shadrack, D.M., Swai, H.S., Munissi, J.J.E., Mubofu, E.B., Nyandoro, S.S., 2018. Polyamidoamine dendrimers for enhanced solubility of small molecules and other desirable properties for site specific delivery: insights from experimental and computational studies. Molecules 23. https://doi.org/10.3390/molecules23061419.

Shah, K.U., Khan, G.M., 2012. Regulating drug release behavior and kinetics from matrix tablets based on fine particle-sized ethyl cellulose ether derivatives: An in vitro and in vivo evaluation. Sci. World J. 2012 https://doi.org/10.1100/2012/842348.

Zaman, M., Butt, M.H., Siddique, W., Iqbal, M.O., Nisar, N., Mumtaz, A., Nazeer, H.Y., Alshammari, A., Riaz, M.S., 2022. Fabrication of PEGylated chitosan nanoparticles containing tenofovir alafenamide: synthesis and characterization. Molecules 27. https://doi.org/10.3390/molecules27238401.

Zhang, L., Zhu, S., Qian, L., Pei, Y., Qiu, Y., Jiang, Y., 2011. RGD-modified PEG-PAMAM-DOX conjugates: In vitro and in vivo studies for glioma. Eur. J. Pharm. Biopharm. 79, 232–240. https://doi.org/10.1016/j.ejpb.2011.03.025.